Dynamical heterogeneity in soft-particle suspensions under shear

K. N. Nordstrom, J. P. Gollub, and D. J. Durian

Phys. Rev. E **84**, 021403 — Published 22 August 2011

DOI: 10.1103/PhysRevE.84.021403

Dynamical heterogeneity in soft particle suspensions under shear

K. N. Nordstrom[1], J. P. Gollub[1,2], and D. J. Durian[1]
[1]*Department of Physics and Astronomy, University of Pennsylvania, Philadelphia, PA 19104-6396, USA and*
[2]*Department of Physics and Astronomy, Haverford College, Haverford, PA 19041-1392, USA*

We present experimental measurements of dynamical heterogeneities in a dense system of microgel spheres, sheared at different rates and at different packing fractions in a microfluidic channel, and visualized with high speed digital video microscopy. A four-point dynamic susceptibility is deduced from video correlations, and is found to exhibit a peak that grows in height and shifts to longer times as the jamming transition is approached from two different directions. In particular, the time for particle-size root-mean square relative displacements is found to scale as $\tau^* \sim (\dot{\gamma}\Delta\phi^4)^{-1}$ where $\dot{\gamma}$ is the strain rate and $\Delta\phi = |\phi - \phi_c|$ is the distance from the random close packing volume fraction. The typical number of particles in a dynamical heterogeneity is deduced from the susceptibility peak height and found to scale as $n^* \sim (\dot{\gamma}\Delta\phi^4)^{-0.3}$. Exponent uncertainties are less than ten percent. We emphasize that the same power-law behavior is found at packing fractions above and below ϕ_c. Thus, our results considerably extend a previous observation of $n^* \sim \dot{\gamma}^{-0.3}$ for granular heap flow at fixed packing below ϕ_c. Furthermore, the implied result $n^* \sim (\tau^*)^{0.3}$ compares well with expectation from mode-coupling theory and with prior observations for driven granular systems.

PACS numbers: 64.70.pv, 83.80.Kn, 05.20.Jj

I. INTRODUCTION

Disordered materials of all kinds are considered to be "jammed" if the relaxation time grows longer than the observation window, so that that the constituent particles appear locked into a fixed configuration of nearest neighbors [1–3]. For example, supercooled liquids can become jammed by lowering the temperature; hard sphere colloidal particles can become jammed by increasing the density; macroscopic glass beads can become jammed by lowering a driving force below some threshold. No matter what the material or set of control parameters, as jamming is approached it has long been assumed that the growing relaxation time is accompanied by increasing co-operativity in particle motion [4]. The closer to jamming, the larger the number of neighbors that must cooperate in order to rearrange and the less frequently this happens.

It is now widely accepted that the rearrangement dynamics are not continuous near jamming, but rather are spatially and temporally heterogeneous [5, 6]. Intermittent string-like swirls of rearranging particles come and go in a background of less mobile particles. The four-point dynamical susceptibility $\chi_4(\tau)$ is a powerful tool for characterizing such dynamical heterogeneities [7, 8]. This function exhibits a peak at a characteristic relaxation time, τ^*, and the peak height χ_4^* can be related by a counting argument to the number n^* of particles in the fast rearranging regions [9]. One of the central questions today, then, is the quantitative relationship between the respective growth of τ^* and of χ_4^* on approach to jamming. Expectations for various models are reviewed in Ref. [8]. For example a logarithmic connection is expected for "collectively-rearranging region" scenarios. A power-law connection $\chi_4^* \propto (\tau^*)^\lambda$ is predicted by mode-coupling theory, where λ is the reciprocal of the mode-coupling exponent, γ; Ref. [8] particularly notes the values $\lambda = 0.37$ [10] and $\lambda = 0.40$ [11]. A power-law connection with $\lambda = 1$ is expected for freely-diffusing defects. And more recently a value $\lambda = 1/2$ was reported for a kinetically constrained model jamming model [12].

For colloidal hard spheres this issue was recently explored in Ref. [13], which improves upon pioneering observations [14–17] by covering an unprecedented density range near jamming such that the structural relaxation time increased by seven orders of magnitude. The data show that τ^* grows faster than a power law, and n^* grows slower than a power law, in $1/(\phi_c - \phi)$ as ϕ approaches ϕ_c from below. The critical packing fraction ϕ_c is close to, but possibly distinct from, random close packing. Irrespective of the value, the conclusion is that n^* grows logarithmically with τ^*. For other colloidal systems it is not yet known whether this relationship depends on the nature of the particle interactions, or whether it changes when the control parameter is temperature or driving rather than just density. In this paper, we report on dynamical heterogeneities for dense suspensions of soft Hertzian colloidal particles. In particular we measure the time and size scales, and determine how they grow as jamming is approached both by bringing the density toward ϕ_c, from either side, and also by lowering the strain rate. In addition to establishing the dependence of n^* and τ^* on these two control parameters, we also show that the size and time scales are related by a power law. This result contrasts with Ref. [13], but compares well with observations for macroscopic hard spherical grains, where the control parameters are density and fluidizing air speed [18] or strain rate and depth into a flowing heap [19]. Here, as in Ref. [13] and Ref. [19], the dynamic range in relaxation time is more than seven orders of magnitude.

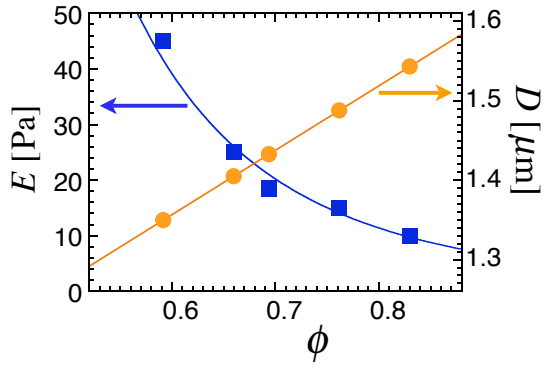

FIG. 1: (Color online) Properties of NIPA microgels as a function of packing fraction, as controlled by temperature: (left) the elastic modulus measured by centrifugal compression, and (right) the particle diameter measured by dynamic light scattering [20].

II. EXPERIMENTAL DETAILS

The system we study is a dense aqueous suspension of thermoresponsive N-isopropylacrylamide (NIPA) microgel beads [21, 22], synthesized with the Yodh group at Penn [23–27]. Dynamical heterogeneities for unsheared suspensions of such particles have been reported previously in Refs. [25, 28, 29], both below random close packing as well as above – where aging effects are important. Here experiments are performed on ≈10% polydisperse suspensions of two different size particles, primarily about 1 μm but also of about 0.6 μm in diameter. For the former, the number density is $0.455/\mu\text{m}^3$ and the viscosity of the suspending water is $\eta_0 = 0.01$ g/(cm · s) = 0.001 Pa · s. Fig. 1 shows the diameter D and Young elastic modulus E for the larger particles, obtained previously from dynamic light scattering and centrifugal compression [20] respectively, as a function of volume fraction ϕ. For decreasing temperature the particles swell with water and soften, so D increases while E decreases. Since the applied pressure needed to squeeze water from the gel is very large compared to the elastic modulus [20], the particles deform without deswelling and can be compressed to a known volume fraction ϕ above random close packing $\phi_c = 0.635$, simply by lowering the temperature. For the chosen fixed number density of the $D \approx 1$ μm sample, the relationship between volume fraction and temperature is accurately described by $\phi(T) = 1.34 - T/(29.4\ ^\circ\text{C})$ over the temperature range $19\ ^\circ\text{C} \le T \le 25\ ^\circ\text{C}$ used here (see Fig. 2 of Ref. [20]).

Previously we studied the shear rheology of these suspensions by a custom microfluidic technique, in which the velocity profile is measured at the mid-height of a tall channel for various packing fractions and for various pressure-controlled flows [30]. The experimental channel is 25 μm wide, 100 μm tall, and $L = 2$ cm long, fabricated of PDMS by soft lithography and bonded to a glass microscope slide. The video imaging system consists of a Phantom CMOS camera (1-10,000 fps) connected to a Zeiss Axiovert 200 microscope with 100× objective. An objective-cooling collar (Bioptechs) and cooling plate above the sample are controlled to about ±0.01 °C (misquoted as 0.1 °C in [30]). This corresponds to a volume fraction control of ±0.0003. The suspension is forced through the channel using pressurized air and inlet/outlet tubing of sufficient diameter that the imposed pressure drop ΔP occurs only along the length L of the channel and can be related to the local shear stress in the suspension as $\sigma(y) = \Delta P y/L$. The local strain rate is found by numerical differentiation of the velocity profile, $\dot{\gamma}(y) = \partial v_x(y)/\partial y$. These two local measures are then combined to give the stress vs strain rate shear rheology. For packing fractions varied discretely between 0.5 and 0.7, and for strain rates varied continuously from nearly 10^{-4} to 100 s^{-1}, we found that the shear rheology data

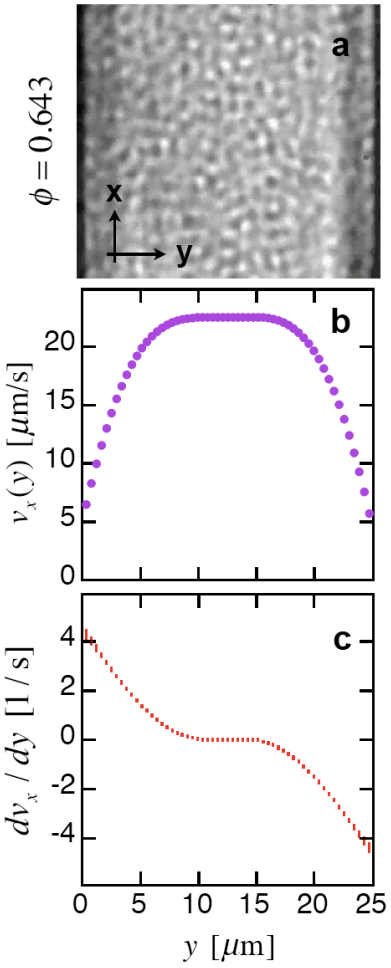

FIG. 2: (Color online) (a) An image taken from video data of particles. (b) The velocity and (c) the strain rate, as a function of position across the channel, averaged over time for a $T = 60$ s run with a PIV delay time of $\tau_p = 50$ ms. In (c) the height of the points is the statistical uncertainty based on the difference between the velocity data and the local cubic polynomial fits used for differentiation.

could be collapsed onto two branches by Olsson-Teitel [31] scaling with powers of the distance $\Delta\phi = |\phi - \phi_c|$ to jamming; the resulting exponents can be understood in terms of particle interactions [32]. In the following sections, we analyze the same data for dynamical heterogeneities.

Since the strain rate is a crucial parameter, we provide further experimental details. An example video frame is displayed in Fig. 2a. The bead-scale intensity variations are insufficient to permit particle tracking, but are ideal for Particle Image Velocimetry (PIV) measurement of the average velocity profile, $v_x(y)$ vs y, where y is measured across the channel and x is in the flow direction. With custom LabVIEW code, the images are broken into fifty strips, 0.5 μm, which is about 7 times the pixel width of $l = 0.07$ μm, and $F = 175$ μm $= 2450l$ pixels long. The speed of each strip is then found by maximizing its spatial cross correlation with an image strip taken at a later time, chosen so that the particle displacement is at least one diameter. Final velocity profiles are obtained by averaging over all video data. Final strain rate profiles are obtained by fitting each profile point and its six neighbors to a cubic polynomial (see supplemental material of Ref. [30]). Note that the the distance over which the differentiation is performed is thus $\delta y = 3$ μm.

Example velocity and strain rate profiles are shown in Figs. 2b-c. There the packing fraction is $\phi = 0.643$, which is above random close packing, $\phi_c = 0.635$. Therefore, the flow is somewhat plug-like and exhibits wall slip. Considering all packing fractions and driving pressures, the range of speeds is $0.04 - 200$ μm/s and the range of strain rates is $3 \times 10^{-4} - 1000$/s. If speeds are measured with an uncertainty of one-tenth percent, for example, then the strain rate uncertainty would be $\Delta\dot\gamma \approx 0.001v/\delta y$, which can be as small as 10^{-5}/s.

An order-of-magnitude estimate of the uncertainty in the strain rate may be made as follows. The PIV delay time, τ_p, is an important input; it ought to be chosen as $\tau_p > D/v$ where D is the particle size and v is the average speed. The speed uncertainty is $\Delta x/\tau_p$ where Δx is the uncertainty in locating the maximum spatial cross-correlation for time-delayed images of one particle-scale blob. If located by fit to a peaked function, then $\Delta x = l/\sqrt{n}$ where l is the pixel size and $n = D/l$ is the number of pixels per blob. For a video data set of duration T, the speed uncertainty is reduced by a factor of $1/\sqrt{N}$ where $N = vT/D$ is the total number of blobs examined. Dividing the speed uncertainty by the transverse distance over which the differentiation is performed, δy, gives the expected scaling of the strain rate uncertainty as

$$\Delta\dot\gamma \;\propto\; \frac{1}{\tau_p \delta y}\sqrt{\frac{l^3}{vT}}, \tag{1}$$

$$<\; \frac{v}{\delta y}\sqrt{\frac{l^3}{vTD^2}}. \tag{2}$$

For our experiments, the pixel size is $l = 0.07$ μm and the differentiation length is $\delta y = 3$ μm. In the example of Fig. 2c, the plotted error bars agree with the right-hand side of Eq. (1) times a factor of about seven. For the smallest strain rates, $\dot\gamma \approx 10^{-4}$/s, the speeds are slower and the run durations are longer: $v \approx 0.04$ μm/s, $T = 2$ hours. For these numbers the right hand side of Eq. (2) is 10^{-5}/s, showing that the measurement is feasible if the PIV delay time is properly chosen.

Lastly, before analyzing for dynamical heterogeneities, we discuss the possibility of a non-uniform volume fraction that could be induced by the variation of strain rate across the width of sample. For hard sphere colloids, even very small concentration gradients can be amplified by shear [33]. However, our system of soft spheres would probably correspond better to an emulsion, where no significant concentration gradient is seen under shear [34]. Indeed, we find no sign of a concentration gradient across the channel, either directly or indirectly. Unfortunately video images could reveal only a gross variation, greater than at least several percent. However, shear rheology data of Ref. [30] indicate that one volume fraction value collapses multiple strain rates (corresponding to multiple positions across the channel) onto a single master curve with two branches. If the volume fraction were significantly nonuniform, this collapse would fail. Judging from the insets of Fig. 4 in Ref. [30], an inhomogeneity in ϕ of 0.005 would be detectable but probably not a change of 0.001.

III. HETEROGENEITY ANALYSIS

While the presence of dynamical heterogeneities can be registered by the correlation of equal-time velocity fluctuations, the use of higher order correlation functions is required to demonstrate that the dynamics are truly heterogeneous in space and time. See for example Refs. [5–7] for reviews. As done for quiescent systems, we thus characterize the spatiotemporally heterogeneous nature of the dynamics using a four-point dynamic susceptibility, $\chi_4(\tau)$, which exhibits a peak that grows in proportion to the size of the heterogeneities. The measurement of $\chi_4(\tau)$ begins with an ensemble-averaged self-overlap order parameter, $Q_t(\tau)$, constructed so that the contribution from each particle decays from 1 toward 0 as time increases from t to $t+\tau$ and the particle moves some prescribed distance. If all particles were to experience the same rearrangement dynamics, then the decay of $Q_t(\tau)$ vs τ would be independent of t. But if the dynamics were heterogeneous, then the decay of $Q_t(\tau)$ would be faster or slower than the time average $Q(\tau) \equiv \langle Q_t(\tau)\rangle$ according to the number of independent rearranging regions that happen to exist at a particular instant. This is governed by counting statistics, so the variance

$$\chi_4(\tau) \equiv N\left[\langle Q_t^2(\tau)\rangle - \langle Q_t(\tau)\rangle^2\right] \tag{3}$$

is independent of the number N of particles in the field of view. The average number n^* of particles in a fast rearranging region has been explicitly computed in Ref. [9]

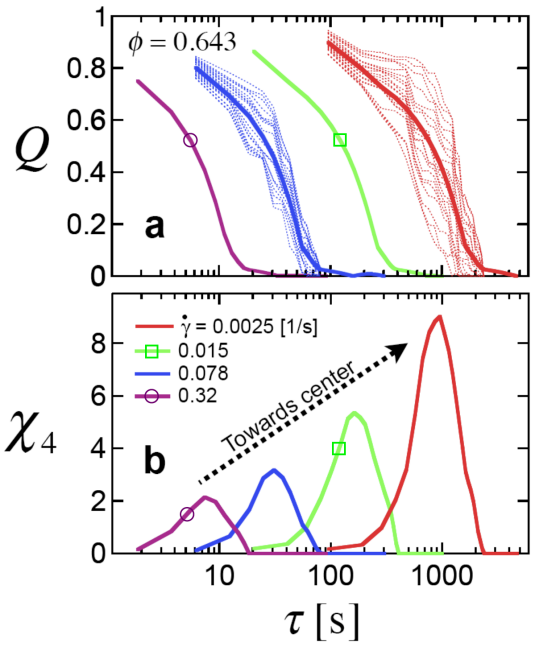

FIG. 3: (Color online) (a) Overlap order parameters and (b) corresponding dynamic susceptibilities, plotted vs delay time for several strain rates as labelled. The packing fraction is $\phi = 0.643$, as in Fig. 2 where strain rates are seen to be lower towards the center of the channel. In (a) the light dashed curves represent $Q_t(\tau)$ for a selection of different start times t, and the heavy solid curves represent the average $Q(\tau) = \langle Q_t(\tau)\rangle$ over all t.

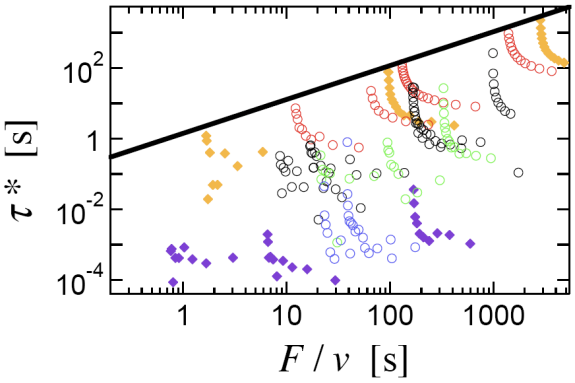

FIG. 4: (Color online) Relaxation time, τ^*, as a function of residence time, F/v, where $F = 175$ μm is the length of the field of view and v is the average velocity of a strip of particles. Since all data are under the black line $\tau^* = F/v$, the timescales probed are less than the channel residence time and hence are not improperly measured. The symbols are the same as in Fig. 6.

as

$$n^* = \frac{\chi_4^*}{(Q_1 - Q_0)(Q_1 - Q^*)} \qquad (4)$$

where $\chi_4^* = \chi_4(\tau^*)$ is the peak height, $Q^* = Q(\tau^*)$, and Q_1 and Q_0 are respectively the average values of the overlap parameter at delay τ^* taken separately over beads in slow and fast rearranging regions. The same results for n^* were found for three very different choices for overlap order parameters, whose associated susceptibilities had different peak heights and peak times: step function, persistent area, persistent bond [9]. Therefore, as long as the prescription of Eq. (4) is followed, the choice of overlap order parameter is not crucial.

Here we use this same standard procedure, implemented in a co-moving frame. Since the video data, as in Fig. 2, have insufficient resolution to track individual particle positions, we adopt an overlap order parameter similar to that introduced in Ref. [19] based on image correlations. In particular, we divide the video images into 50 narrow strips of constant speed and strain rate, 7 pixels ≈ 0.5 μm wide, containing $N \approx 200$ particles. For each of these strips we compute

$$Q_t(\tau) \equiv \frac{\langle I_i(t) I_{i+\mathrm{d}i}(t+\tau)\rangle - \langle I_i(t)\rangle^2}{\langle I_i(t)^2\rangle - \langle I_i(t)\rangle^2} \qquad (5)$$

where $\langle\cdots\rangle$ is the ensemble average over all pixels i running along a row, where $\mathrm{d}i = v\tau/l$, and where l is the pixel size. This is done for each of the seven rows of pixels in each strip, and averaged together. Since $i+\mathrm{d}i$ is not an integer, the value of $I_{i+\mathrm{d}i}$ is taken by interpolation of the intensity at pixels with indices above and below $i+\mathrm{d}i$. Prior to this, the speed v of the strip was found by varying $\mathrm{d}i$ at fixed τ, and averaging over t, to maximize the cross-correlation as in the usual PIV method. Note that the length scale probed by the associated four-point susceptibility is set by the particle-size grayscale variations in the video images. Therefore the time τ^* at which $\chi_4(\tau)$ reaches its peak is a characteristic relaxation time needed for particle-scale relative displacements. For illustration, example results for $Q_t(\tau)$ vs τ are shown in Fig. 3a for a strip corresponding to packing fraction $\phi = 0.643$ and strain rate $\dot{\gamma} = 0.0025$ s^{-1}. This is close to jamming, and indeed the decay is quite variable. Multiplying the variance by N gives the susceptibility shown in Fig. 3b. This exhibits a peak at delay time $\tau^* \approx 1000$ s of height $\chi_4^* \approx 9$, when the average overlap order parameter is $Q^* \approx 0.5$. For a second example strip with a higher strain rate, $\dot{\gamma} = 0.078$ s^{-1}, the dynamics are more homogeneous as seen in Fig. 3 by the tighter spread of $Q_t(\tau)$ and the smaller susceptibility. As a final check, Fig. 4 shows a plot of τ^* vs channel residence time F/v, where F is the length of the field of view and v is average particle speed. All of the data fall below the line of equality, $\tau^* = F/v$, showing that the relaxation time is smaller than the residence time and hence is not improperly measured.

To deduce the number n^* of particles in a fast rearranging region from the peak height χ_4^* using Eq. (4), we must first find the three different averages of the overlap order parameter at delay time τ^*. These are shown in Fig. 5 as a function of volume fraction, where each point corresponds to a different strip and hence to a different

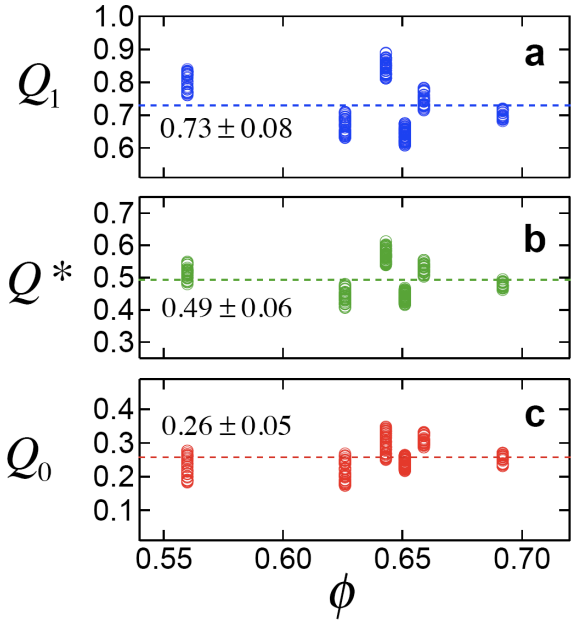

FIG. 5: (Color online) Averages of the overlap order parameter at time delay τ^*, plotted versus volume fraction, where each data point represents a different strain rate: (a) Q_1 and (c) Q_0 are the averages for the slow and fast rearranging regions, respectively, whereas (b) $Q* = Q(\tau^*)$ is the average for the whole sample. None of these quantities is found to depend on volume fraction or strain rate; their averages are indicated by the dashed horizontal lines with accompanying values.

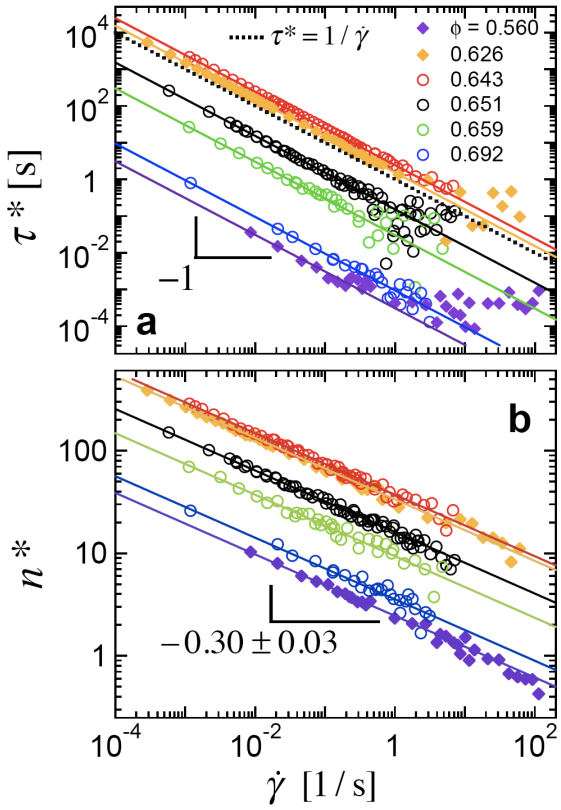

FIG. 6: (Color online) (a) Relaxation time and (b) number of particles in a fast-rearranging heterogeneity, plotted versus strain rate, for several volume fractions ϕ as labelled. The solid lines are fits to a power of $\dot{\gamma}$, with exponents of -1 in (a) and of -0.3 in (b).

strain rate. Since there is no evident variation with volume fraction, or strain rate, we simply compute a total average over all conditions. The average overlap order parameter at the time τ^* when χ_4 peaks is found to be $Q^* \equiv Q(\tau^*) = 0.49 \pm 0.06$. The average for beads in the slow rearranging regions, i.e. for beads with order parameter greater than Q^*, is $Q_1 = 0.73 \pm 0.08$. The average for the fast rearranging regions, i.e. for beads with order parameter less than Q^*, is $Q_0 = 0.26 \pm 0.05$. These three averages are indicated by dashed horizontal lines in Fig. 5. Note that the constancy of Q_1, Q_0, and Q^* implies that the factor of N in the Eq. (3) definition of $\chi_4(\tau)$ is not significantly affected by the flow of beads into and out of the field of view.

Since the overlap order parameter is measured in a long strip, about half a particle wide and 200 particles long, the field of view may not contain the entirety of any of the fast rearranging regions. However if the heterogeneities are 1-dimensional string-like swirls, as expected for a quiescent system, then they will cut the field of view a number of times in proportion to their length. Therefore, the true number of particles involved would be a constant multiplicative factor larger than the n^* value we deduce by the above prescription. This is borne out by the good comparison of the size of heterogeneities in a monolayer of air-fluidized beads, analyzed across the whole sample or in strips [35]. But it could also be that in channel flow the heterogenieties are linear chains or sheets of particles aligned with the velocity, in which the true number of particles involved would still be proportional to the n^* value we deduce.

IV. RESULTS

Data for the relaxation time τ^* and the number n^* of particles in a fast-rearranging region are plotted vs strain rate in Figs. 6a-b, respectively, for the ~ 1 μm diameter colloidal microgel particles. There, each data set corresponds to a given packing fraction as labelled, and each data point corresponds to a different strip and hence to a different strain rate. As the strain rate decreases and jamming is approached, both τ^* and n^* grow as powers of the strain rate. For the time scale, the power law is consistent with $\tau^* \propto 1/\dot{\gamma}$ as shown by the solid lines. This is the simplest dimensionally-correct possibility. For the size scale, all power law fits are consistent with $n^* \propto 1/\dot{\gamma}^{0.30 \pm 0.03}$. This exponent agrees with recent observations of a value near 1/3 in dry granular systems,

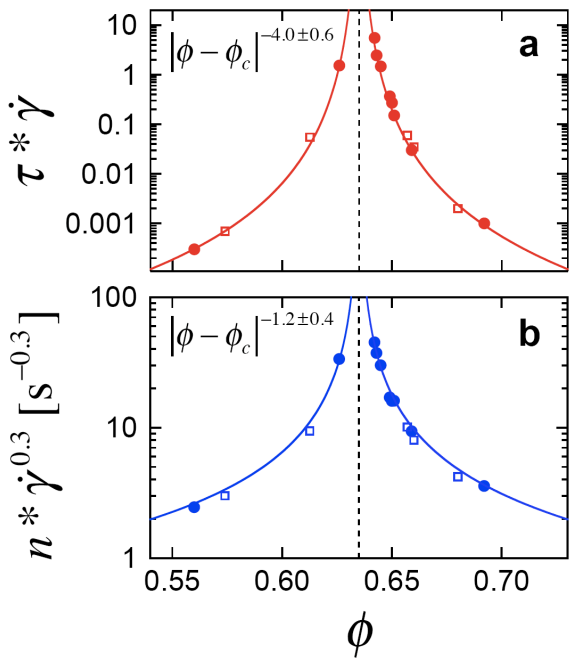

FIG. 7: (Color online) Coefficients of the fits in Fig. 6 to (a) $\tau^* \propto 1/\dot\gamma$ and (b) $n^* \propto 1/\dot\gamma^{0.3}$ vs volume fraction, shown as closed symbols, for the ~ 1 μm diameter particles. The open symbols are for the smaller ~ 0.6 μm diameter particles. The solid curves are fits to a power of $\Delta\phi \equiv |\phi - \phi_c|$, where $\phi_c = 0.635$ is the random close packing fraction, with exponents of -4 in (a) and of -1.2 in (b).

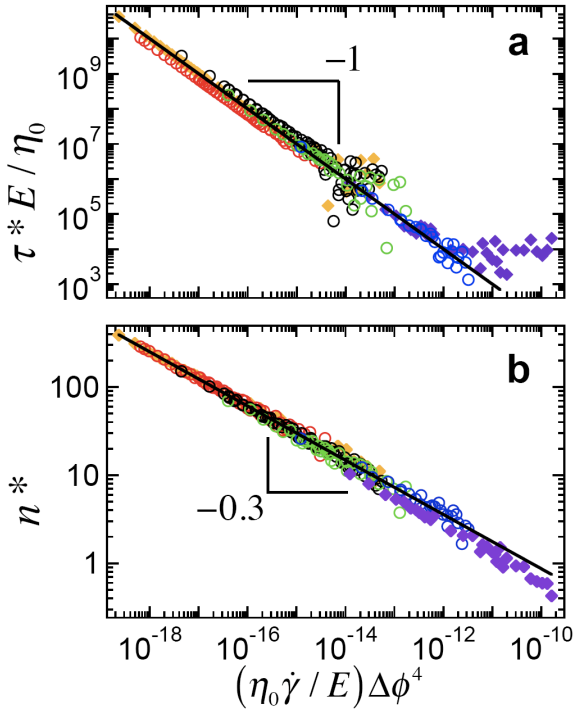

FIG. 8: (Color online) Scaling collapse of (a) dimensionless relaxation time and (b) number of particles in a fast-rearranging heterogeneity versus dimensionless strain rate times $\Delta\phi \equiv |\phi - \phi_c|$ to the fourth. Here η_0 is the viscosity of water and E is the Young elastic modulus of the particulate material. The symbol types are the same as in Fig. 6. The solid lines are power-laws with exponents as labeled; these fit well except for a noticeable deviation at the largest strain rates.

including experiments on heap flow [19], simulations of uniform shear [36], and simulations of flow down an incline [37]. In these works, shear occurs at essentially fixed packing fraction near ϕ_c. A value in the range $0.2 - 0.3$ was also reported for a Lennard-Jones system [38]. So our observations considerably reinforce and extend all these results, not just to overdamped systems but also to packing fractions away from ϕ_c both above and below. Nonetheless, the value of approximately 1/3 has yet to be explained.

The relaxation time and number of particles in a fast-rearranging region also depend on packing fraction, as well as strain rate. This can be seen already in Figs. 6a-b, where the data sets shift up and then down as ϕ goes from below to above ϕ_c. This is displayed more clearly in Fig. 7a-b, where the coefficients $\tau^*\dot\gamma$ and $n^*\dot\gamma^{0.3}$ of the power law fits in the previous figure are plotted vs ϕ. The results grow without apparent bound as ϕ_c is approached from either side. Data for the smaller particles are also included, and display the same behavior. These divergences are well described by fits to power laws in $\Delta\phi = |\phi - \phi_c|$, as shown, giving $\tau^* \propto 1/\Delta\phi^{4.0\pm0.6}$ and $n^* \propto 1/\Delta\phi^{1.2\pm0.4}$.

Altogether we thus find that the relaxation time and the size of fast-rearranging heterogeneities grow as the jamming transition is approached as functions of strain rate and packing fraction as

$$\tau^* \propto (\dot\gamma\Delta\phi^4)^{-1}, \quad (6)$$
$$n^* \propto (\dot\gamma\Delta\phi^4)^{-0.3}. \quad (7)$$

Notice that the combination $(\dot\gamma\Delta\phi^4)$ controls the behavior in both cases. Hence there is more sensitivity to variation of $\Delta\phi$ than to variation of strain rate. This is qualitatively consistent with numerical results for a driven kinetically constrained jamming model [12]. To emphasize this feature, we plot all τ^* and n^* results versus $(\dot\gamma\Delta\phi^4)$ in Figs. 8a-b, where $\dot\gamma$ is rendered dimensionless by the intrinsic time scale set by the ratio η_0/E of liquid viscosity to particle modulus. Note that this collapses the data onto power laws with exponents -1 and -0.3, respectively. Thus, there are only three exponents to explain rather than four. As discussed already, the -1 makes dimensional sense and the -0.3 extends prior observations but is not understood. The remaining exponent, 4, is reminiscent of the exponent $\Gamma = 4$ in the timescale $\eta_0/(E\Delta\phi^\Gamma)$ used in Olsson-Teitel scaling plots of the shear rheology [30].

We note that some prior results are inconsistent with Eqs. (6-7). In Ref. [38] a simulated Lennard-Jones system

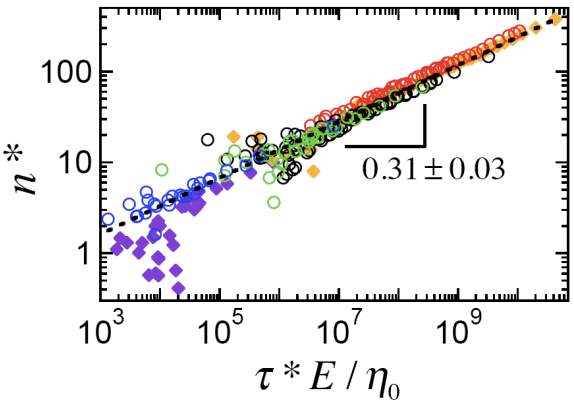

FIG. 9: (Color online) Number n^* of particles in a fast-rearranging heterogeneity vs relaxation time τ^*, made dimensionless by the Young modulus E of the particulate material and the viscosity η_0 of the suspending fluid (water). The dashed black line is a power-law fit with exponent $\lambda = 0.31 \pm 0.03$ as labeled. The symbol types are the same as in Fig. 6

shows the same size scaling, $\chi_4^* \sim 1/\dot{\gamma}^{0.3}$, but a different relaxation time scaling, $\tau^* \sim 1/\dot{\gamma}^{0.5}$. In Ref. [39] simulated harmonically-repulsive particles under quasistatic shear show $\chi_4^* \sim 1/\Delta\phi^{1.8}$; the system at nonzero strain rates [40] shows $\chi_4^* \sim 1/\dot{\gamma}^{0.5-0.7}$, though the dependence on strain rate may not be a power law. In Ref. [41], relaxation time data for a sheared hard sphere glass were found to scale as $\tau^* \sim 1/\dot{\gamma}^{0.8}$. And in Ref. [42], relaxation time data for a sheared monolayer of bubbles were found to scale as $\tau^* \sim 1/\dot{\gamma}^{0.66}$. The cause of these discrepancies with our results is unclear, but cannot be ascribed to use of a co-moving frame since $\tau^* \sim 1/\dot{\gamma}$ was observed in Ref. [19] where the overlap order parameter was computed in the lab frame.

V. DISCUSSION

The observations made here, summarized by Eqs. (6-7), combine to give the size of heterogeneities as a power-law of the relaxation time:

$$n^* \propto (\tau^*)^{\lambda}. \tag{8}$$

For emphasis, we plot n^* data vs $\tau^* E/\eta_0$ in Fig. 9 on logarithmic axes and observe that indeed the data collapse to a straight line, except for one data set whose noise blooms at small $\tau^* E/\eta_0$. Note that the dynamic range of the data is more than two decades in size and nearly eight in dimensionless relaxation time, which is sufficient to rule out the possibilities of a logarithmic or exponential connection between n^* and τ^*. Fitting to a power-law gives the exponent and uncertainty as

$$\lambda = 0.31 \pm 0.03. \tag{9}$$

The observed power-law form is consistent with mode-coupling theory [8], and the observed exponent is only slightly smaller than the expectation $\lambda = 1/\gamma$ where γ is the mode-coupling exponent [10, 11].

One advantage of plotting n^* and τ^* parametrically versus one another, rather than versus the control parameters, is that it allows comparison with other systems where there is no shear or where the control parameter is something other than strain rate. For example, $\lambda = 1/2$ is reported for the driven kinetically constrained model mentioned above [12], while a logarithmic connection better accounts for the simulations of Brownian harmonically-repulsive particles [43]. In terms of experiment, comparison is possible for only a few experiments of which we are aware. For hard spheres, Ref. [13] found that τ^* grows faster than a power law, and that χ_4^* grows slower than a power law, as ϕ approaches ϕ_c from below. It is stated that n^* grows logarithmically with τ^*, which disagrees with our results. However, the final five decades may be reasonably fit with $\lambda = 1/3$. For soft NIPA microgel particles similar to those studied here, Ref. [28] found that both τ^* and χ_4^* grow with increasing packing fraction; no functional form was proposed or tested. We digitized their data and plot parametrically, rather than vs packing fraction, and find power law behavior of the form Eq. (8) with exponent $\lambda = 0.34 \pm 0.16$. This is consistent with our findings. For a monolayer of large spherical grains fluidized by a steady upflow of air, Ref. [18] found that there is a meaningful effective temperature $T_{\rm eff}$, and that size and time scales are consistent with $n^* \sim 1/{T_{\rm eff}}^{0.7\pm0.2}$ and $\tau^* \sim 1/{T_{\rm eff}}^{2\pm0.5}$, respectively. These combine to give a power law relationship, Eq. (8), with exponent $\lambda = 0.35 \pm 0.15$ that agrees with the results here in Fig. 9. Further experiments on the fluidized grains, where the sample is tilted and where the analysis is carried out by dividing the sample into a series of strips each at a different pressure, also appear to agree [35]. For steady gravity-driven flow of grains down along a confined heap, and visualized through the sidewalls as a function of depth z below the free surface, Ref. [19] found $\tau^* \propto 1/I$ and $n^* \propto (1/I)^{\lambda}$ where $I = \dot{\gamma} d/\sqrt{gz}$ is the inertia number, d is the grain diameter, $g = 9.8$ m/s^2, and $\lambda = 0.33 \pm 0.02$. This system is underdamped, so the time scale is rendered dimensionless by different microscopic physics, but the exponent for the power-law connection between n^* and τ^* is the same as found here.

VI. CONCLUSION

In this paper we presented a study of dynamical heterogeneities in a colloidal system that (a) is not hard spheres, (b) is compressed above as well as below ϕ_c, and (c) is subjected to shear. Our experiments made crucial use of custom synthesized NIPA microgel particles and of a custom fabricated microfluidic channel, as well as of a novel video-based dynamical order parameter. As jamming is approached by bringing the packing fraction difference $\Delta\phi = |\phi - \phi_c|$, or the strain rate $\dot{\gamma}$, to zero, we demonstrated that the time and size scales for dynamical

heterogeneities both grow as powers of the combination $(\dot{\gamma}\Delta\phi^4)$ according to Eqs. (6-7). While there is precedent for the observed strain rate dependence from experiments on underdamped granular systems, the packing fraction dependence appears to be a new result. The observed connection between the size and time scale is a power law, $n^* \propto (\tau^*)^\lambda$, consistent with mode coupling theories but perhaps not with observations for an unsheared suspension of Brownian hard sphere colloids. It is intriguing that the exponent we find, $\lambda \approx 1/3$, agrees with precedents for unsheared soft particles [28] and for two driven systems of hard grains – one with shear [19] and one without [18, 35]. This suggests universality with respect to interactions, but perhaps with unsheared hard sphere colloids in a different universality class.

This work was supported by the National Science Foundation through grants MRSEC/DMR05-20020 and DMR-0704147. We thank L. Cipelletti, A.J. Liu, and P. Yunker for helpful conversations. We thank A. Alsayed, A. Basu, and Z. Zhang for their help in synthesizing the particles.

[1] A. J. Liu and S. R. Nagel, eds., *Jamming and Rheology: Constrained Dynamics on Microscopic and Macroscopic Scales* (Taylor and Francis, New York, 2001).
[2] C. S. O'Hern, L. E. Silbert, A. J. Liu, and S. R. Nagel, Phys. Rev. E **68**, 011306 (2003).
[3] A. J. Liu and S. R. Nagel, Ann. Rev. Cond. Matt. Phys. **1**, 347 (2010).
[4] G. Adam and J. H. Gibbs, J. Chem. Phys. **43**, 139 (1965).
[5] L. Berthier, G. Biroli, J.-P. Bouchaud, L. Cipelletti, and W. van Saarloos, eds., *Dynamical heterogeneities in glasses, colloids, and granular media* (Oxford University Press, 2011).
[6] L. Berthier, Physics **4**, 42 (2011).
[7] N. Lacevic, F. W. Starr, T. B. Schroder, and S. C. Glotzer, J. Chem. Phys. **119**, 7372 (2003).
[8] C. Toninelli, M. Wyart, L. Berthier, G. Biroli, and J. P. Bouchaud, Phys. Rev. E **71**, 041505 (2005).
[9] A. R. Abate and D. J. Durian, Phys. Rev. E **76**, 021306 (2007).
[10] W. Kob and H. C. Andersen, Phys. Rev. Lett. **73**, 1376 (1994).
[11] S. Whitelam, L. Berthier, and J. P. Garrahan, Phys. Rev. Lett. **92**, 185705 (2004).
[12] Y. Shokef and A. J. Liu, Europhys. Lett. **90**, 6 (2010).
[13] G. Brambilla, D. El Masri, M. Pierno, L. Berthier, L. Cipelletti, G. Petekidis, and A. B. Schofield, Phys. Rev. Lett. **102**, 085703 (2009).
[14] A. Kasper, E. Bartsch, and H. Sillescu, Langmuir **14**, 5004 (1998).
[15] A. H. Marcus, J. Schofield, and S. A. Rice, Phys. Rev. E **60**, 5725 (1999).
[16] W. K. Kegel and A. van Blaaderen, Science **287**, 290 (2000).
[17] E. R. Weeks, J. C. Crocker, A. C. Levitt, A. Schofield, and D. A. Weitz, Science **287**, 627 (2000).
[18] A. R. Abate and D. J. Durian, Phys. Rev. Lett. **101**, 245701 (2008).
[19] H. Katsuragi, A. R. Abate, and D. J. Durian, Soft Matter **6**, 3023 (2010).
[20] K. N. Nordstrom, E. Verneuil, W. G. Ellenbroek, T. C. Lubensky, J. P. Gollub, and D. J. Durian, Phys. Rev. E **82**, 041403 (2010).
[21] B. R. Saunders and B. Vincent, Adv. Coll. I. Sci. **80**, 1 (1999).
[22] R. Pelton, Adv. Coll. I. Sci. **85**, 1 (2000).
[23] A. M. Alsayed, M. F. Islam, J. Zhang, P. J. Collings, and A. G. Yodh, Science **309**, 1207 (2005).
[24] Z. X. Zhang, N. Xu, D. T. N. Chen, P. Yunker, A. M. Alsayed, K. B. Aptowicz, P. Habdas, A. J. Liu, S. R. Nagel, and A. G. Yodh, Nature **459**, 230 (2009).
[25] P. Yunker, Z. X. Zhang, K. B. Aptowicz, and A. G. Yodh, Phys. Rev. Lett. **103**, 115701 (2009).
[26] P. Yunker, Z. X. Zhang, and A. G. Yodh, Phys. Rev. Lett. **104**, 015701 (2010).
[27] K. Chen, W. G. Ellenbroek, Z. X. Zhang, D. T. N. Chen, P. J. Yunker, S. Henkes, C. Brito, O. Dauchot, W. van Saarloos, A. J. Liu, et al., Phys. Rev. Lett. **105**, 025501 (2010).
[28] D. A. Sessoms, I. Bischofberger, L. Cipelletti, and V. Trappe, Phil. Trans. Roc. Soc. A **367**, 5013 (2009).
[29] R. Colin, A. M. Alsayed, J.-C. Castaing, R. Goyal, L. Hough, and B. Abou, Soft Matter **7**, 4504 (2011).
[30] K. N. Nordstrom, E. Verneuil, P. E. Arratia, A. Basu, Z. Zhang, A. G. Yodh, J. P. Gollub, and D. J. Durian, Phys. Rev. Lett. **105**, 175701 (2010).
[31] P. Olsson and S. Teitel, Phys. Rev. Lett. **99**, 178001 (2007).
[32] B. P. Tighe, E. Woldhuis, J. J. C. Remmers, W. van Saarloos, and M. van Hecke, Phys. Rev. Lett. **105**, 088303 (2010).
[33] R. Besseling, L. Isa, P. Ballesta, G. Petekidis, M. E. Cates, and W. C. K. Poon, Phys. Rev. Lett. **105**, 268301 (2010).
[34] J. Goyon, A. Colin, G. Ovarlez, A. Ajdari, and L. Bocquet, Nature **454**, 84 (2008).
[35] L. J. Daniels, T. K. Haxton, N. Xu, A. J. Liu, and D. J. Durian, in preparation (2010).
[36] T. Hatano, arXiv:0804.0477 (2008).
[37] L. Staron, P.-Y. Lagrée, C. Josserand, and D. Lhuillier, Phys. Fluids **22**, 113303 (2010).
[38] M. Tsamados, Eur. Phys. J. E **32**, 165 (2010).
[39] C. Heussinger, L. Berthier, and J. L. Barrat, Europhys. Lett. **90**, 20005 (2010).
[40] C. Heussinger, P. Chaudhuri, and J. L. Barrat, Soft Matter **6**, 3050 (2010).
[41] R. Besseling, E. R. Weeks, A. B. Schofield, and W. C. K. Poon, Phys. Rev. Lett. **99**, 028301 (2007).
[42] M. E. Möbius, G. Katgert, and M. van Hecke, Europhys. Lett. **90**, 44003 (2010).
[43] T. K. Haxton and A. J. Liu, Europhys. Lett. **90**, 66004 (2010).